Pergamon

Int. J. Heat Mass Transfer. Vol. 40, No. 6, pp. 1481–1490, 1997

0017–9310/97 $17.00+0.00

PII: S0017–9310(96)00069–5

Impingement heat transfer and recovery effect with submerged jets of large Prandtl number liquid—I. Unconfined circular jets

C. F. MA, Q. ZHENG and S. C. LEE
Beijing Polytechnic University, Beijing 100022, People's Republic of China

and

T. GOMI
Sophia University, Tokyo 102, Japan

(*Received for publication* 7 *March* 1996)

Abstract—Experimental study was performed to characterize recovery factor and heat transfer coefficient on vertical heaters impinged by submerged circular transformer oil jets issued from both pipe and orifice nozzles. Radial distributions of local recovery factor were determined at various Reynolds numbers and nozzle-to-plate spacings, and compared with numerical result. Local Nusselt number at stagnation point was found to be proportional nearly to square root of jet Reynolds number in the range of $Re = 220$–1500, and essentially unaffected by nozzle-to-plate spacing for $Re < 600$. In total, 32 radial profiles of local heat transfer were obtained with pipe and orifice nozzles. An empirical formula was developed for correlating the local heat transfer data. Unusual variations of Nusselt number with Reynolds number were observed in stagnation zone with Reynolds number around 1300 at $z/d = 16$ and 20. Through numerical integration average heat transfer was determined and correlated. Copyright © 1996 Elsevier Science Ltd.

1. INTRODUCTION

Cooling of heated surfaces of high heat flux by impinging liquid jets has become an established technique [1]. The applications of this high performance technique are wide ranging and include oil jets in liquid-cooled internal combustion engines [2], fluorocarbon and water jets in advanced computers [3] and water jets in hot rolling process of metals [4]. Many investigations on heat transfer under impinging submerged [5–12] and free surface [13–18] circular liquid jets have been published. These studies have focused largely on Prandtl number range from 2 to 25 with water [11, 17], freon [6, 9], fluorocarbon [5, 12, 14] and kerosene [8] as the working fluid. Almost all the experiments in the above works were performed with the impinging jets of which their flow pattern at the nozzle exit was fully turbulent. Only the studies of Metzger *et al.* [18], Gu *et al.* [7] and Ma *et al.* [10] were conducted by circular liquid jets with Prandtl numbers between 70 and 260, and penetrated the range where the jets were initially laminar ($Re < 2000$). More recently, local heat transfer with initially laminar circular water jets were investigated by Elison and Webb [19] in low Reynolds number range. Some unusual thermal behavior was discovered. Further research is needed to explore the heat transfer characteristics with large Prandtl number liquid jets at initially laminar regime.

It has been testified by Metzger *et al.* [18] and Ma *et al.* [10] for large Prandtl number liquid jets that the difference between the target surface temperature and the adiabatic wall temperature, instead of the difference between the surface temperature and the jet static temperature, should be used in the calculation of heat transfer coefficient even at relatively lower jet velocity. If the temperature difference between the wall and the jet was very large, the recovery effect would be unimportant. However, most jet impingement heat transfer tests, including the present work, were performed with the temperature difference approx 10 K. In consequence, information of local recovery factor is needed to evaluate the heat transfer coefficient. Knowledge of adiabatic temperature is of great importance for applications of the measured heat transfer results. To the best knowledge of the present authors, the local characteristics of recovery factor have not been reported for impinging liquid jets in open literature.

Using transformer oil as the test liquid, experiments were performed in this work with submerged jets issued from both pipe and orifice nozzles of 1 mm (normal) in diameter at jet velocities up to 23 m s^{-1}. The present experimental study was carried out in the ranges of $Re = 220$–1450 and $Pr = 170$–280.

The first objective of this work was to characterize the local recovery factor with submerged circular jets of large Prandtl number liquid. Radial distributions

NOMENCLATURE

A	area of heated surface, empirical constant
B	empirical constant
C	empirical constant
C_p	specific heat at constant pressure
d	jet nozzle diameter
h	local heat transfer coefficient
I	current intensity
k	thermal conductivity
m	empirical constants
$\underline{Nu}$	$h \cdot d/k$, local Nusselt number
$\overline{Nu}$	average Nusselt number
n	empirical constants
Pr	$C_p\mu/k$, Prandtl number
p	empirical constants
q	heat flux
r	recovery factor
R	radial coordinate, electrical resistance
Re	$u \cdot d/v$, Reynolds number
T_{aw}	adiabatic wall temperature
T_j	jet static temperature at nozzle exit
T_w	wall temperature
u	mean fluid velocity at nozzle exit
z	nozzle-to-plate spacing.

Greek symbols

μ	dynamic viscosity
v	kinematic viscosity
ξ	integral value.

Superscript

$\overline{\ }$	average values.

Subscript

0	stagnation point.

of local recovery factor were measured for various working conditions. The effects of Reynolds number and nozzle-to-plate spacing were examined experimentally in detail. The experimental data were compared with numerical result.

The second objective of this work was to investigate the local heat transfer characteristics with transformer oil jets at low Reynolds number. The influence of the spacing, Reynolds number and nozzle configuration on local heat transfer was examined in experimental detail. In total, 32 profiles of local heat transfer were experimentally determined at various Reynolds numbers and spacings. Most of them were well correlated. Based on the local measured results, average heat transfer coefficient was also obtained and correlated.

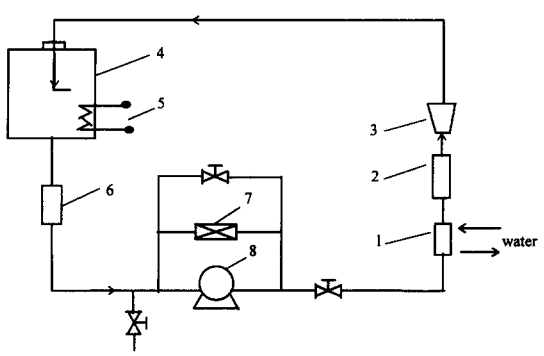

Fig. 1. Schematic layout of flow loop. 1, Cooler; 2, electrical heater; 3, flow meter; 4, test chamber; 5, auxiliary heater; 6, filter; 7, by-pass valve; 8, pump.

2. EXPERIMENTAL APPARATUS AND METHOD

The test liquid in this study was transformer oil. The working fluid was circulated in a closed loop which had provision for filtering, metering, preheating, and cooling as shown in Fig. 1. The test chamber was constructed of stainless steel with three visual ports as illustrated in Fig. 2. A flexible polyethylene tube joined the two sections of the chamber cover. The test section assembly was vertically fixed on one side of the chamber. The details of the test section assembly are presented in Fig. 3. The main part was a strip of 10 μm thick constantan foil with a heated section of 5 mm $\times$ 10 mm (nominal) exposed to the coolant. The strip on either side of this active section was welded to copper bus blocks, which were in turn connected to power leads. The heated section of the foil was cemented to a backlite block inserted between copper blocks. The assembly was cemented in Plexiglass disk fixed in a brass housing with a screwed flange. The test section was highly insulated in thermal design by fiberglass to minimize heat loss. The temperature of the center of the inner surface of the heater was measured by a 40 gage iron–constantan thermocouple which was electrically insulated from the foil yet in close thermal contact. The active section of the constantan foil was used as an electrically heating element as well as a heat transfer surface. Alternating current power to the test section was provided by a 50 A power supply. The intensity of the current through the test section was measured by an ammeter.

The oil jets issued from a horizontal jet tube of 0.987 mm inside diameter and 35 mm length. Using the large length-to-diameter ratio tube, a fully developed laminar pipe flow can be obtained at nozzle exit. As shown in Fig. 4. the fluid was supplied from a vertical delivery tube to the jet nozzle passing a plenum box of 125 cm^3. Both the jet tube and the

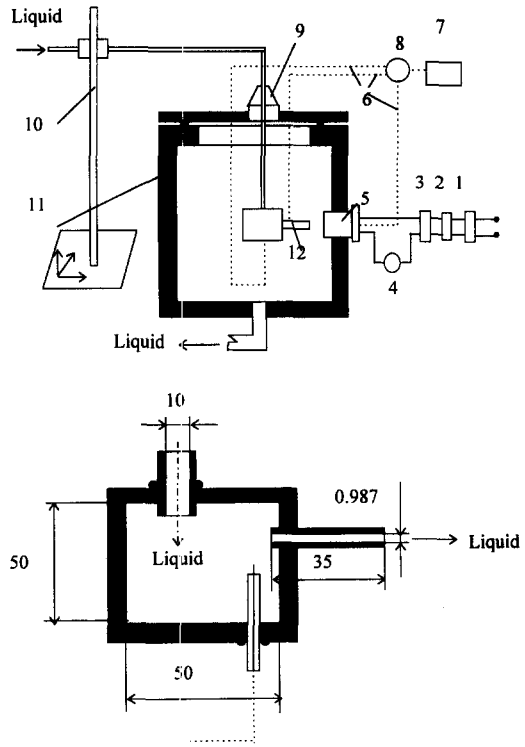

Fig. 2. Details of test chamber and instrumentation. 1, Stabilized voltage supply; 2, voltage regulator; 3, voltage transformer; 4, ammeter; 5, test section assembly; 6, thermocouples; 7, MV meter; 8, switch; 9, flexible plastics; 10, three-dimensional coordinate frame; 11, chamber; 12, jet tube.

delivery tube were made of stainless steel and fixed with the plenum box. Their axes were perpendicular with each other in a vertical plane. The jet tube-delivery tube assembly was fixed on a three-dimensional coordinate rack and could be adjusted with respect to the test section with placements accomplished with ± 0.01 mm. The jet temperature was measured by a 40 gage iron–constantan thermocouple placed inside the plenum box close to the entrance of the jet tube. In the range of jet velocity investigated in this work, the difference between the jet static and total temperatures can be neglected. In order to study the effect of the nozzle geometry, experiments were also performed with an orifice-type nozzle that was a round hole of 1.048 mm diameter made in a brass plate of 1 mm thickness. Due to the flexible nature of the plastic seal at the top of the test chamber, the pressure in the chamber is considered close to the atmosphere.

In preliminary experiments the jet tube was oriented perpendicularly to the test section. The distance between the nozzle and the target surface was accurately adjusted by means of the three-dimensional frame. In order to ensure that the nozzle centerline coincided with the midpoint of the heater, a procedure of centering was developed whereby the jet was moved on the heated surface until minimum wall temperature was recorded by the thermocouple. The measured wall temperature at the heater center was taken as the local value. By recording this temperature for various locations of the jet tube, the horizontal temperature distributions could be obtained for given jet conditions and surface heat flux. Properties of the working fluid were evaluated at the film temperature by averaging the wall and jet temperatures. In the experiments the temperature of the jets and the fluid in the container were accommodated with each other so that their difference could be less than 1 K for eliminating the effect of ambient fluid entertainment into the impinging jets in the heat transfer process.

The area of the heated surface was carefully measured for each test section assembly with a tool maker's microscope of 0.001 mm resolution. Heat flux was calculated from the electrical power supplied to the test section and the area of one side of the heated surface. Heat flux was determined by the following formula:

$$q = \frac{I^2 R}{A} \tag{1}$$

where the resistance R was measured accurately with direct current before experiments. It was verified in preliminary tests that the variation of the resistance with temperature could be neglected (less than $\pm 0.1\%$), as the heater temperature variation is less than 55 K in the present study and the variation in resistivity with temperature is extremely small for constantan.

In order to calculate the heat transfer coefficient the recovery factor should be obtained by

$$r = \frac{T_{aw} - T_j}{u^2/2C_p} \tag{2}$$

In this work the radial distribution of the adiabatic wall temperature on the target surface was measured at constant jet velocity when the surface heat flux was zero. Then, the radial profile of recovery factor was determined by equation (2) as a function of jet Reynolds number, nozzle-to-plate spacing and fluid Prandtl number.

The uncertainty in Nusselt number was influenced primarily by the determination of heat flux and wall temperature. The surface heat flux was affected by the variation of the constantan foil thickness that was claimed in the supplier's specification to be less than 3% of the normal value. This value is taken as the indicator of heat flux variation due to foil thickness nonuniformity. Preliminary experiments were performed to check heat loss from the heater, and indicated that with jet impingement the maximum conduction loss to the back of the heater assembly was less than 0.8% of the power put into the heater. This conclusion was supported by a conduction analysis for this study. So, no correction was included for such conduction loss in this work. The determination of the

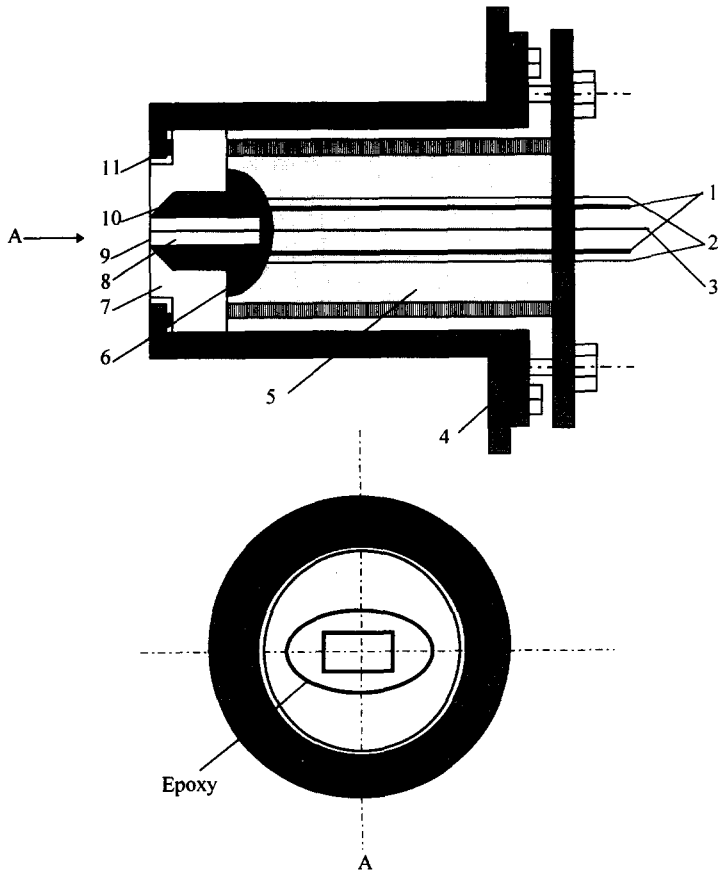

Fig. 3. Details of electrically heated test section. 1, Power lead; 2, voltage tap; 3, thermocouple; 4, tank wall; 5, fiberglass; 6, epoxy; 7, Plexiglass; 8, bakelite; 9, 10 μ thick constantan foil; 10, copper block; 11, O-ring.

heater surface temperature was related to the thermal resistance of the adhesive layer between the thermocouple bead and the back side of the foil. During the manufacture process the foil strip was strongly suppressed to the top surface of the bakelite block to minimize the thickness of the adhesive layer in between. Measurements were made of the adhesive thickness with several used test sections after their failure in experiments. The thickness was determined between 0.04 and 0.1 mm. As the conduction heat loss was less than 0.8% of the power input, and its main part passed through the bus bars, the uncertainty arising from position of the thermocouple bead was estimated to be always less than 0.15 K in this study. Another source of the uncertainty in wall temperature was concerned with lateral heat conduction along the constantan foil caused by the sharp radial variation of the heat transfer coefficient around the stagnation zone. Using the measured wall temperature distribution, this uncertainty was determined to be negligible (less than 0.5%) due to the extremely small thickness of the foil. All the thermocouples were calibrated to an accuracy of ± 0.1 K before experiments. The uncertainty in Nusselt number was determined to be less than $\pm 5\%$. The uncertainty in Reynolds number was affected by the measurement of the flowrate and the nozzle exit area. While the flow meter was carefully calibrated, the nozzle exit area was precisely determined using the tool maker's microscope of 0.001 mm resolution. The uncertainty in Reynolds number did not exceed $\pm 5.5\%$.

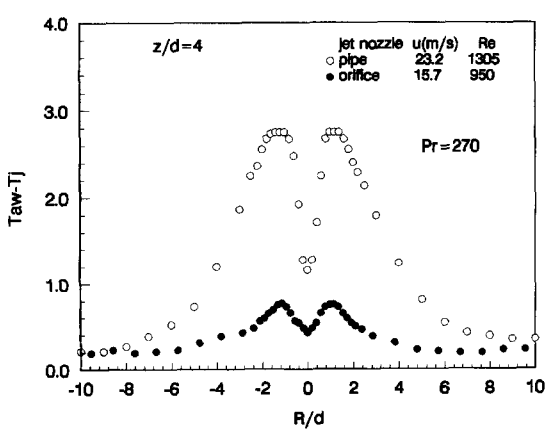

Fig. 4. Radial variation of adiabatic wall temperature.

3. RESULTS AND DISCUSSION

3.1. *Recovery factor*

Some typical results of recovery temperature at different Reynolds numbers for the two nozzle configurations are presented in Fig. 4. It is noted for the profiles that with higher jet velocity the two peaks of the temperature difference $(T_{aw} - T_j)$ reach about 3 K near the stagnation point. Apparently, negligence of the recovery effect will result in very significant error in the case of the present work. Radial distributions of local recovery factor were measured at constant spacing $z/d = 4$ corresponding to different Reynolds numbers. The experimental results are presented in Fig. 5. All the profiles exhibit a humped shape with two peaks symmetrically to the stagnation point located at about $R/d \approx 1.5$. Between the two humps a minimum appears at the stagnation point. Beyond the two peaks the factor decreases monotonically with the radial distance. The recovery factor is seen to be insignificantly influenced by Reynolds number from Fig. 5. Slight dependence of recovery factor on Reynolds number was also observed by Goldstein *et al.* [20] for circular air jets. Figure 6 indicates the effect of nozzle-to-plate spacing on recovery factor. Significant influence of the spacing was observed both for the two types of nozzles. As shown in Figs. 6 (a) and (b), the streamwise recovery factor distributions drop with increasing of the nozzle-to-plate spacing. But the figures exhibit good similarity in the curve shapes of the recovery factor profiles at various spacings. Two humps were observed for all the profiles at similar locations. Two profiles of similar Reynolds number presented in Figs. 5 and 6 (b), respectively are plotted again in Fig. 7 to highlight the difference in the recovery factor distribution between the orifice and pipe type nozzles at same axial location. As shown in the figure the recovery factor for the orifice nozzle is significantly lower than for the pipe nozzle in both stagnation and wall jet zones. The two profiles indicate similar characteristics of the recovery factor variations. The complexity and lack of detailed knowledge of the impingement liquid flow prevent convincing explanation for this behavior.

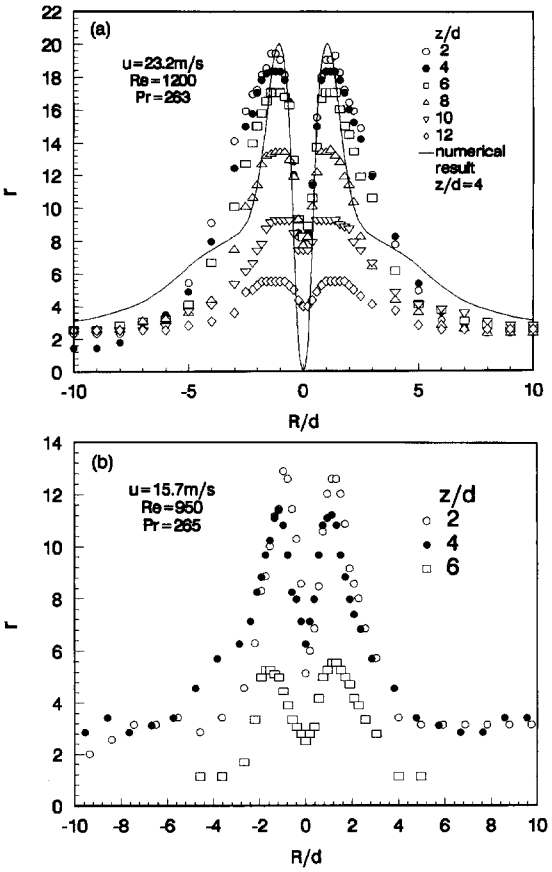

Fig. 6. Radial distribution of the recovery factor at different nozzle-to-plate spacings: (a) pipe-type nozzle; (b) orifice-type nozzle.

To the best knowledge of the present authors, detailed information of recovery factor is not available in open literature for impinging submerged liquid jets. However, systematically experimental study has been conducted with circular air jets by Goldstein *et al.* [20]

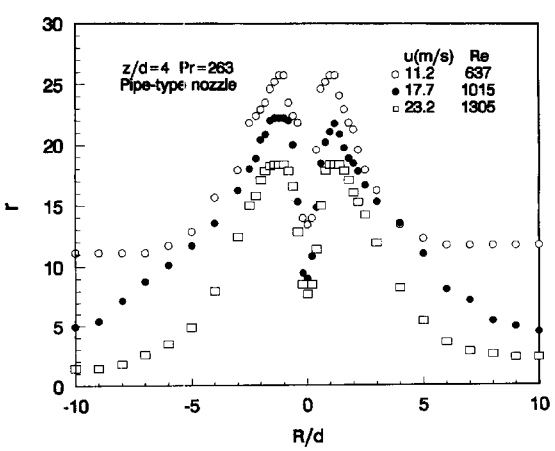

Fig. 5. Radial distribution of the recovery factor for various Reynolds numbers.

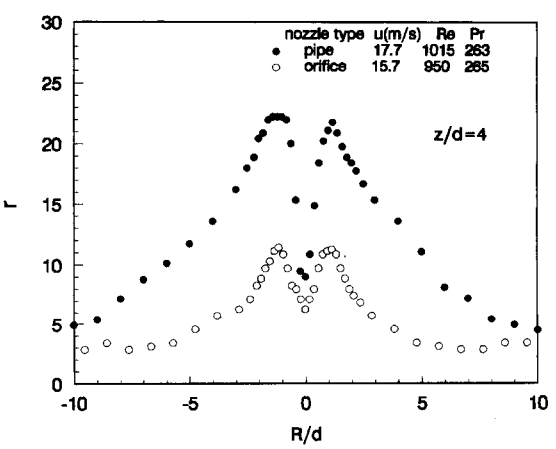

Fig. 7. Comparison of the radial distribution of the recovery factors between the pipe-type and orifice-type nozzles.

in the range of Reynolds number between 61 000 and 124 000. Streamwise distribution of local recovery factor was obtained. The effect of Reynolds number and nozzle-to-plate spacing was studied experimentally. Because of the great difference in Prandtl number and Reynolds number, it seems difficult to get meaningful result from comparison between the two investigations. A numerical study is being conducted by the present authors to investigate the local characteristics of recovery factor and heat transfer coefficient with impinging submerged circular jets of transformer oil. This work will be published. The numerical recovery factor result of $z/d = 4$ is presented in Fig. 6 in comparison with the experimental data. In general, the agreement of the experimental result is quite good with the numerical study. Both the experimental and numerical curves of recovery factor display a local minimum at stagnation point and two local maxima symmetric to the stagnation point at similar locations as shown in the figure. The only discrepancy between the numerical and experimental results is the value of the local minimum at stagnation point. Zero value was obtained by the numerical work. But the experimental results were much above zero. This discrepancy can be explained by the fact that the thermocouple junction fixed on the target wall was about 0.08 mm. In reality, the experimental data of recovery factor obtained in this work is not exactly a local value but an average one over a small range of $\Delta R \approx 0.1d$.

3.2. *Stagnation point heat transfer*

Effect of nozzle-to-plate spacing on stagnation point heat transfer was carefully examined for both of the two nozzles. The results are presented in Fig. 8. As illustrated by the four curves of lower Reynolds number in the figures, independence of stagnation point heat transfer on the nozzle-to-plate spacing is testified in the range of $Re = 254$–640. This unusual heat transfer phenomenon is consistent with the result that was first reported by Elison and Webb [19] for submerged circular water jets issuing from pipe-type nozzle at Reynolds number less than 800. The independence was attributed to higher transport characteristics of the circular jets after destabilization [19]. In contrast, the two curves of higher Reynolds number (1473 and 1232 for pipe and orifice nozzles, respectively) in the figures exhibit a negligible influence of the spacing inside the so-called potential core, and a considerable decay in the heat transfer rate beyond it. This trend has been reported for initially turbulent liquid jets of water [11, 19] and R113 [9]. It is seen from Fig. 8 that the dimensionless potential core lengths are very different between the two nozzles. Values of 2 and 12 are approximately determined for orifice and pipe-type nozzles, respectively.

The effect of jet Reynolds number on stagnation Nusselt number was investigated experimentally with the plate held at various nozzle-to-plate spacings. The experimental data for pipe and orifice nozzles are plotted in Fig. 9 (a) and (b), respectively. It was found

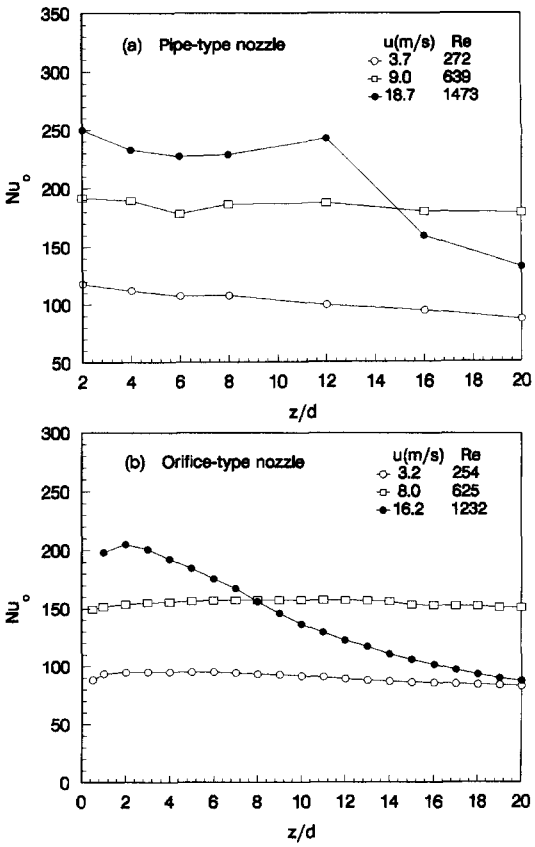

Fig. 8. Variation of stagnation Nusselt number with the nozzle-to-plate spacing at constant Reynolds number: (a) pipe-type nozzle; (b) orifice-type nozzle.

that all the data within the potential core could be well expressed by the correlation

$$Nu = C\,Re^m Pr^{1/3} \tag{3}$$

where the standard Prandtl number exponent of 1/3 was adopted from the recommendation of Ref. [10], and the coefficients C and m were determined from experimental data: $C = 1.46$, $m = 0.471$ for pipe nozzle, and $C = 1.26$, $m = 0.468$ for orifice nozzle. These empirical constants are very close to the values of $C = 1.29$ and $m = 1/2$ reported in Ref. [10]. Equation (3) presents 91 and 100% of all the experimental data inside potential core within $\pm 10\%$ for the pipe and orifice nozzles, respectively. The exponent of Reynolds number clearly indicates the laminar characteristic of the impingement flow in stagnation zone, where the favorable pressure gradient parallel to the target surface tends to laminarize the jet flow. Good agreement is seen from Fig. 9 of equation (3) with the experimental data, both for the two nozzles. If comparison is made between Fig. 9 (a) and (b), it will be found that the present data with the pipe nozzle are about 13% higher than those with the orifice nozzle. As shown in the figures, the former expectantly agree well with the correlation proposed by Ma *et al.*

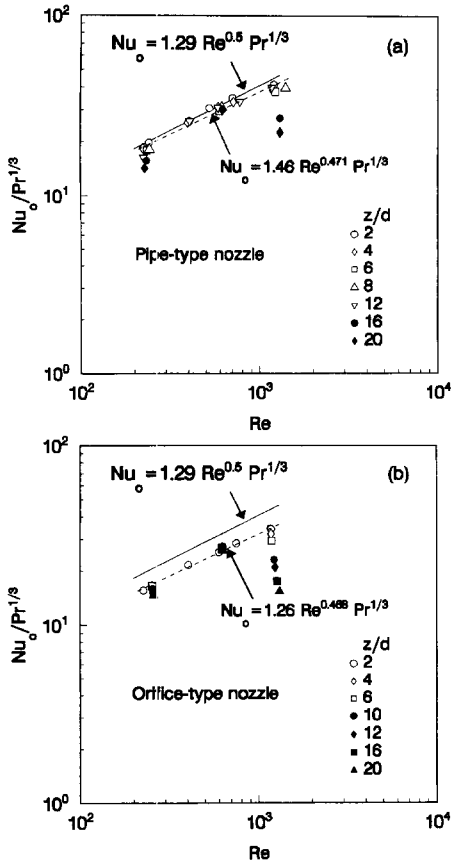

Fig. 9. Variation of stagnation Nusselt number with jet Reynolds number at constant spacing: (a) pipe-type nozzle; (b) orifice-type nozzle.

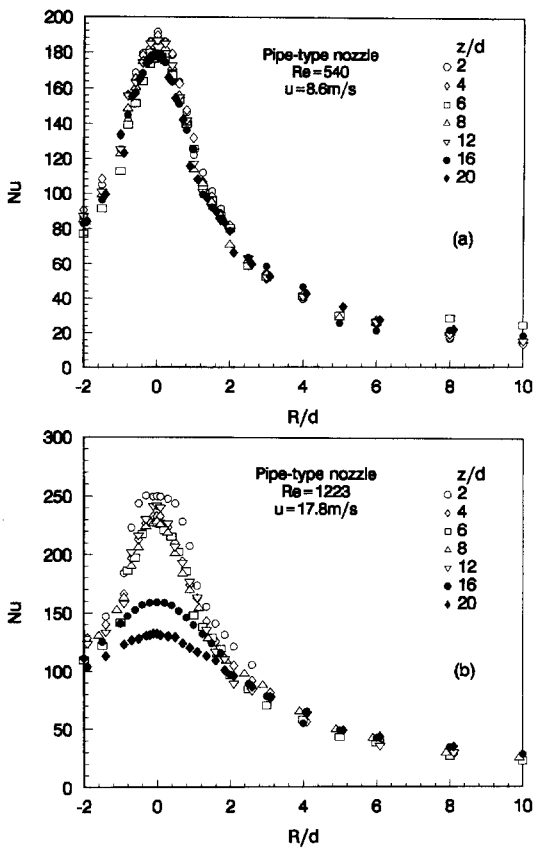

Fig. 10. Radial profiles of local heat transfer at constant jet Reynolds number: (a) $Re = 540$; (b) $Re = 1223$.

[10] for pipe-type nozzle, while the later lower about 20% than the correlation.

With the target held beyond the potential core the characteristics of impingement heat transfer become more complicated. For the initially laminar jets with $Re < 640$, the stagnation Nusselt number is negligibly affected by the spacing. For the case of $Re > 1000$, the impinging jets might be at initially transitional regime, and increase of jet Reynolds number results in reduction of Nusselt number with the target held far beyond the potential core. As displayed by the solid symbols in Fig. 9 (a) and (b), a distinct trend is observed with the experimental data of $z/d \geqslant 16$ (for pipe nozzle) or 10 (for orifice nozzle) that the increase of Reynolds number over about 1000 brings the stagnation Nusselt number down even lower than those corresponding to $Re < 1000$. This anomalous variation will be discussed in more detail in the following section.

3.3. *Radial profile of local heat transfer*

Radial variation of local heat transfer was studied experimentally. In total 32 profiles were obtained in the range of $Re = 220 \sim 1447$ and $z/d = 2$–20. Twenty seven profiles were measured with the pipe-type nozzle. Only five profiles were obtained with the orifice nozzle. The local heat transfer was measured as a function of radial distance from the stagnation point, nozzle-to-plate spacing and jet Reynolds number.

Figure 10 indicates the effect of the spacing on radial distribution of local heat transfer. As shown in Fig. 10 (a), the local heat transfer profiles are not affected by the spacing at lower Reynolds number. All the seven profiles in the figure are nearly identical with each other in the range of $z/d = 2 \sim 20$. All the radial profiles display a bell shape: a maximum occurs at stagnation point, then decreases monotonically along the radial distance. For higher Reynolds number, as illustrated in Fig. 10 (b), the profiles are essentially not influenced by the spacing inside the potential core ($z/d \leqslant 12$). But with the target held beyond $z/d = 12$ the profiles become planar with decreasing maxima at the stagnation point.

The effect of Reynolds number may be very different, depending on the nozzle-to-plate spacing. With the target held within the potential core, increase of Reynolds number elevates the distribution curves of local heat transfer coefficient at a constant spacing. Figure 11 (a) illustrates this normal variation of Nusselt number profile with Reynolds number. With the target held beyond the potential core, unusual radial variation phenomenon was observed at $z/d = 16$ and 20 as shown in Fig. 11 (b) and (c), respectively. The

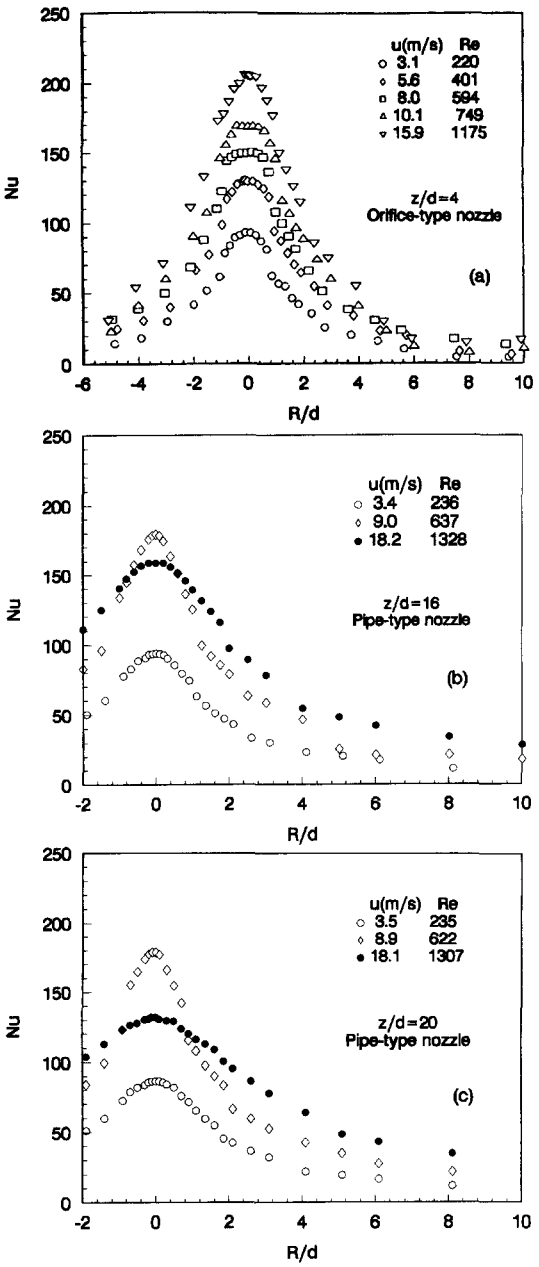

Fig. 11. Radial profiles of local heat transfer at constant spacing: (a) orifice-type nozzle, $z/d = 4$; (b) pipe-type nozzle, $z/d = 16$; (c) pipe-type nozzle, $z/d = 20$.

heat transfer coefficients corresponding to $Re \approx 1300$ are up to 11.4% and 26.3% lower than those associated with $Re \approx 600$ in the stagnation zones of $R/d < 0.7$ and 0.9 for $z/d = 16$ and 20, respectively. Beyond these regimes the curves for $Re \approx 1300$ are above those for the lower Re number. It is also seen from the figures that the two curves for the higher Reynolds number exhibit far less variation with radial distance. The anomalous variation is more pronounced at $z/d = 20$ than $z/d = 16$. The above result is consistent with that stated in the last section. This non-monotonic variation of Nusselt number with jet Reynolds number was also reported by Elison and Webb [19] for submerged circular water jets with $Re = 2600$–2900 at $z/d = 20$. This unusual behavior probably is due to the heat transfer enhancement by turbulence intensity resulted from destabilization of the laminar submerged jets at low Reynolds number. Further explanation of this complex problem is precluded by the lack of detailed information concerning the impingement flow.

An attempt was made to develop an empirical formula to correlate the local heat transfer profiles. It was found that most local heat transfer coefficients may be well correlated after normalization to the stagnation point coefficients by the following equation

$$\frac{Nu}{Nu_0} = \frac{1}{1 + A(R/d)^n} \tag{4}$$

where the empirical constants were determined using a least-squares technique from the experimental data. The values of A and n were obtained to be 0.340 and 1.75 for pipe type nozzle, and 0.199 and 2.13 for orifice type nozzle respectively.

As shown in Fig. 12, good agreement is observed between equation (4) and all the measured local heat transfer data with the exception of the two profiles of $Re \approx 1300$ at $z/d = 16$ and 20 presented in Fig. 12 (e). For the 30 radial profiles, equation (4) correlates 82 and 85% of the experimental data within $\pm 15\%$ in the range of $R/d \leqslant 10$ for pipe and orifice nozzles respectively. The average error of equation (4) is ± 9.9 and $\pm 11.5\%$ for pipe and orifice nozzles, respectively.

3.4. *Average heat transfer*

The local heat transfer distributions obtained in this work were numerically integrated to determine the radial profiles of average heat transfer rates. The numerical integration was performed using the following formula for constant-heat-flux surface [20]

$$\overline{Nu} = \frac{R^2}{2\int_0^R \frac{\xi \, d\xi}{Nu}} \tag{5}$$

The integral result for the orifice nozzle is presented in Fig. 13 (a) after normalization to stagnation Nusselt number. It is seen from the figure that all the radial profiles of local average heat transfer are characteristic of bell shape with maximum at stagnation point. All the average values may be well correlated by a formula of the same form as equation (4).

$$\frac{\overline{Nu}}{\overline{Nu_0}} = \frac{1}{1 + B(R/d)^p} \tag{6}$$

where the coefficients were determined from the experimental data: $B = 0.106$ and $p = 2.05$ for orifice type nozzle, and $B = 0.226$ and $p = 1.52$ for pipe type nozzle. Equation (6) presents 82 and 75% of the experimental data within $\pm 15\%$ for pipe and orifice type nozzles respectively. The average error of the cor-

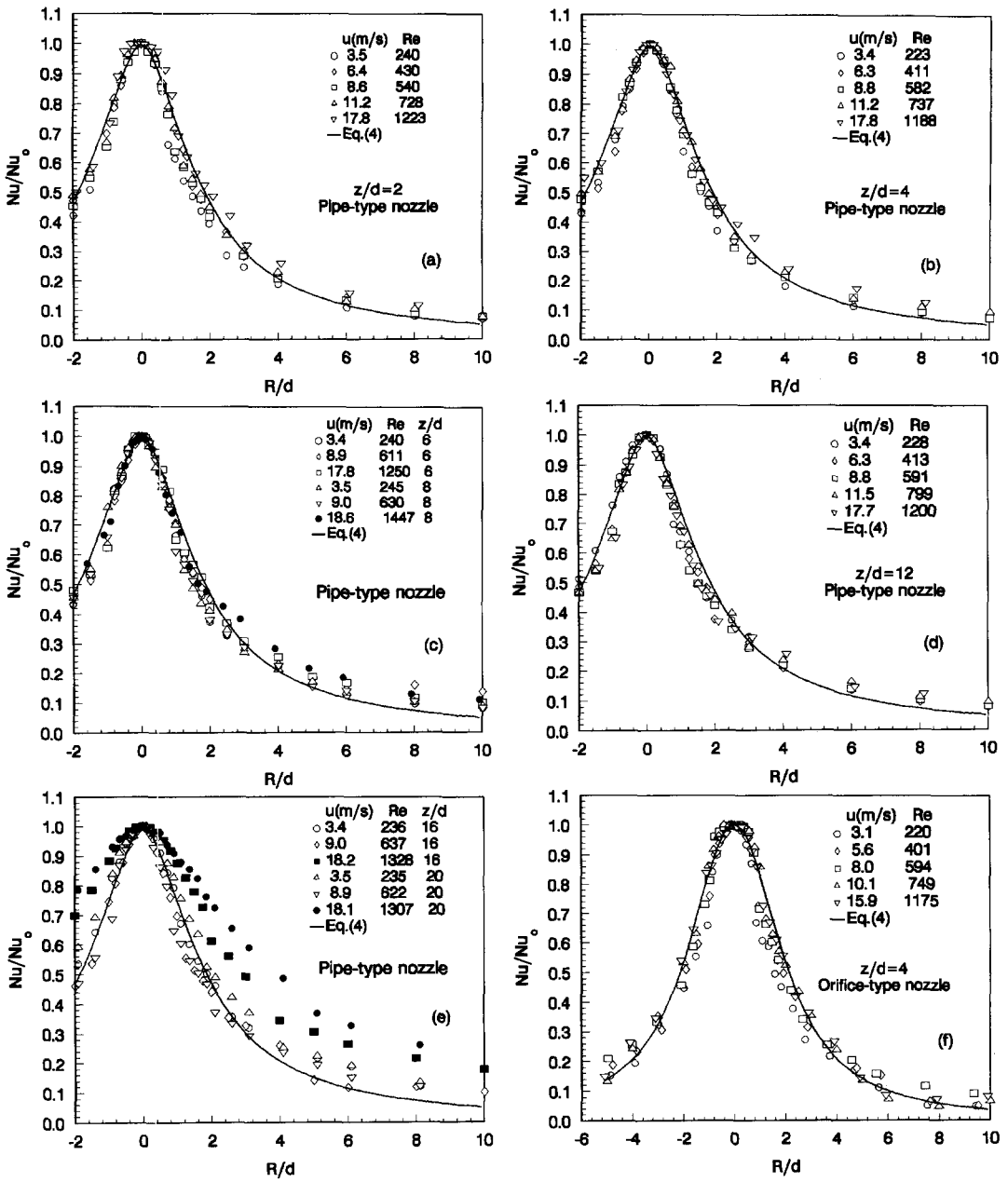

Fig. 12. Correlation of profiles of local heat transfer coefficient: (a) pipe-type nozzle, $z/d = 2$; (b) pipe-type nozzle, $z/d = 4$; (c) pipe-type nozzle, $z/d = 6$ and 8; (d) pipe-type nozzle, $z/d = 12$; (e) pipe-type nozzle, $z/d = 16$ and 20; (f) orifice-type nozzle, $z/d = 4$.

relation is ± 8.6 and $\pm 11.4\%$ for pipe and orifice nozzle, respectively. Agreement is seen from Fig. 13 (a) between the correlation and the orifice nozzle data. Comparison of the correlation with the pipe-type data, precluding those for $Re \approx 1300$ at $z/d = 16$ and 20, is given in Fig. 13 (b), where the vertical bars indicate the data spread.

4. CONCLUSIONS

(1) An extensive and consistent study was carried out to explore recovery effect and to characterize local heat transfer with impinging submerged circular jets of transformer oil issued from pipe and orifice nozzles of 1 mm (nominal) in diameter with jet velocity ranging from 3 to 23 m s^{-1}.

(2) Radial distributions of recovery factor was first measured and reported with large Prandtl number liquid jets in experimental detail. Good agreement of the experimental data with numerical result is observed.

(3) With the target held within the potential core, all the experimental data of stagnation Nusselt number can be well correlated by equation (3). The

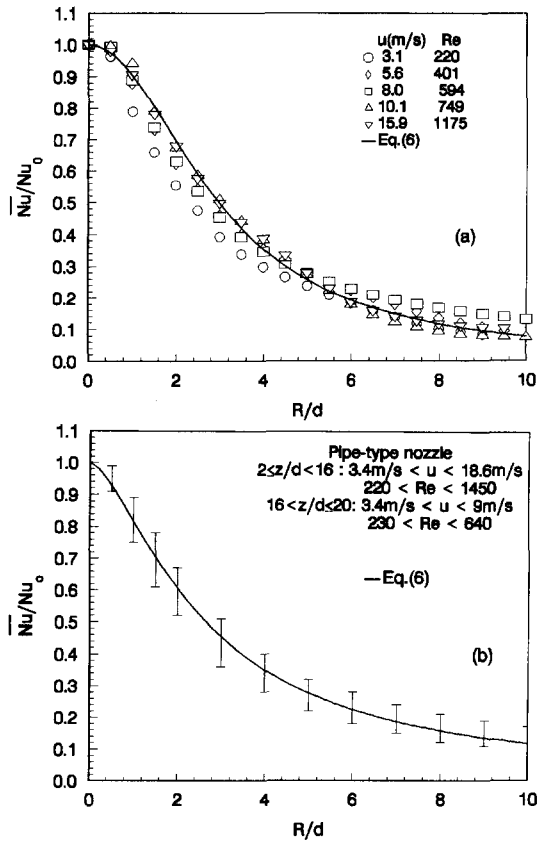

Fig. 13. Correlation of average heat transfer coefficient: (a) orifice-type nozzle; (b) pipe-type nozzle.

exponent of Reynolds number in the correlation clearly suggests the laminar characteristics of the impingement flow in the stagnation zone in the range of $Re = 220 \sim 1500$.

(4) At total, 32 radial profiles of local heat transfer were obtained both with pipe and orifice nozzles. Thirty of them can be well correlated by equation (4). Integral average heat transfer coefficients were obtained and well expressed by equation (6).

(5) Anomalous variations of local Nusselt number were observed with jet Reynolds number around 1300 at $z/d = 16$ and 20. This observation is consistent with that reported in ref. [19] for submerged circular water jets.

Acknowledgements—Support for this work from the National Natural Science Foundation of China is gratefully acknowledged. The authors are grateful to D. H. Lei and Y. Q. Tian for their assistance in this work and to S. Y. Ko and W. X. Qin for their valuable suggestions.

REFERENCES

1. B. W. Webb and C.-F. Ma, Single phase liquid jet impingement heat transfer. *Adv. Heat Transfer*, **26,** 105–217 (1995).
2. M. Kiryu, Development of oil-cooled 750 cc motorcycle engine, *Auto. Technol.* **40,** 1154–1158 (in Japanese) (1986).
3. H. Yamamoto, Y. Udagawa and M. Suzuki, Cooling system for FACOM M-780 large scale computer, In *Proceedings of the International Symposium on Cooling Technology for Electronic Equipment*, pp. 701–714, Pacific Institute for Thermal Engineering (1987).
4. F. C. Kohing, Waterwall: water cooling systems, *Iron Steel Eng.* **62,** 30–36 (1985).
5. D. L. Besserman, F. P. Incropera and S. Ramadhyni, Heat transfer from a square source to an impinging liquid jet confined by annular wall, *J. Heat Transfer* **114,** 284–287 (1992).
6. C. T. Chang, G. Kocamustafaogullari, F. Landis and S. Downing, *Single and Multiple Liquid Jet—Impingement Heat Transfer*, HTD Vol. 246, pp. 43–52. ASME, New York (1993).
7. C. B. Gu, G. S. Su, L. C. Chow and M. R. Pais, Single-phase heat transfer characteristic of submerged jet impingement cooling. AIAA Paper 93-HT-22 (1993).
8. C.-F. Ma, Y. C. Tien, H. Sun, D. H. Lei and A. E. Bergles, Local characteristics of heat transfer from vertical small heater to impinging round jet of liquid of larger *Pr* number. In *Heat Transfer Enhancement and Energy Conservation* (Edited by S. J. Deng), pp. 223–229. Hemisphere, New York (1990).
9. C.-F. Ma and A. E. Bergles, Convective heat transfer on a small vertical heated surface in an impingement circular liquid jet. In *Heat Transfer Science and Technology*—1988 (Edited by B. X. Wang), pp. 193–200. Hemisphere, New York (1988).
10. C.-F. Ma, H. Sun, H. Auracher and T. Gomi, Local convective heat transfer from vertical heated surfaces to impinging circular jets of large Prandtl number fluid, *Proceedings of 9th International Heat Transfer Conference*, Vol. 2, pp. 441–446 (1990).
11. H. Sun, C.-F. Ma and W. Nakayama, Local characteristics of convective heat transfer from simulated microelectronic chips to impinging submerged round water jets, *ASME J. Electron. Packaging* **115,** 71–77 (1993).
12. D. J. Womac, S. Ramadhyani and F. P. Incropera, Correlating equations for impingement cooling of small heat surfaces with single circular liquid jets, *ASME J. Heat Transfer* **115,** 106–115 (1993).
13. S. Faggiani and W. Grassi, Impingement liquid jets on heat surface. In *Proceedings of the 9th International Heat Transfer Conference*, Vol. 1, pp. 275–285 (1990).
14. L. M. Jiji and Z. Dagan, Experimental investigation of single phase multi-jet impingement cooling of an array of microelectronic heat sources. In *Proceedings of the International Symposium on Cooling Technology for Electronic Equipment*, pp. 265–283. Pacific Institute for Thermal Engineering (1987).
15. X. Liu, J. H. V. Lienhard and J. S. Lombara, Convective heat transfer by impingement of circular liquid jets. *J. Heat Transfer* **113,** 571–582 (1991).
16. J. Stevens and B. W. Webb, Local heat transfer coefficients under an axisymmetric, single-phase liquid jet, *J. Heat Transfer* **113,** 71–78 (1991).
17. Y. Pan, J. Stevens and B. W. Webb, Effect of nozzle configuration on transport in the stagnation zone of axisymmetric, impinging free-surface liquid jets—II. Local heat transfer. *J. Heat Transfer* **114,** 880–886 (1992).
18. D. E. Metzger, K. N. Cummings and W. A. Ruby, Effects of Prandtl number on heat transfer characteristics of impinging liquid jets. In *Proceedings of 5th International Heat Transfer Conference*, Vol. 2, pp. 20–24. Hemisphere, Washington (1974).
19. B. Elison and B. W. Webb, Local heat transfer to impinging liquid jets in the initially laminar, transitional, and turbulent regimes. *Int. J. Heat Mass Transfer* **37,** 1207–1216 (1994).
20. R. J. Goldstein, A. I. Behbahani and K. K. Heppelman, Streamwise distribution of the recovery factor and the local heat transfer coefficient to an impinging circular air jet, *Int. J. Heat Mass Transfer* **29,** 1227–1235 (1986).